Quantum control of electron and nuclear spin qubits in the solid-state

M. V. Gurudev Dutt, L. Childress, E. Togan, J. M. Taylor, L. Jiang, A. S. Zibrov, P. R. Hemmer, F. Jelezko, J. Wrachtrup, and M. D. Lukin

Citation: AIP Conference Proceedings **869**, 119 (2006); doi: 10.1063/1.2400641
View online: http://dx.doi.org/10.1063/1.2400641
View Table of Contents: http://scitation.aip.org/content/aip/proceeding/aipcp/869?ver=pdfcov
Published by the AIP Publishing

Quantum control of electron and nuclear spin qubits in the solid-state

M.V. Gurudev Dutt*, L. Childress*, E. Togan*, J. M. Taylor*, L. Jiang*, A.S. Zibrov*, P. R. Hemmer†, F. Jelezko**, J. Wrachtrup** and M. D. Lukin*

*Department of Physics and Institute for Quantum Science and Engineering, Harvard University, Cambridge, MA 02138, USA
†Department of Electrical and Computer Engineering, Texas A&M University, College Station, TX 77843, USA
**Physikalisches Institut, Universtitat Stuttgart, Pfaffenwaldring 57 D-70550 Stuttgart, Germany

Abstract. We review our recent work towards extending quantum control techniques developed in AMO physics to manipulate quantum systems in the solid-state. These systems feature a number of unique opportunities and difficult challenges. Specifically we describe our efforts toward understanding and controlling the complex environment of solid-state quantum bits, coupling them over macroscopic distances as well as ideas for scaling to multi-qubit systems.

Keywords: quantum control, quantum information, color centers
PACS: 76.30.-v,76.60.-k,76.60.Lz,72.25.Rb

INTRODUCTION

The controlled, coherent manipulation of quantum-mechanical systems is an important challenge in modern science and engineering [1]. Solid-state quantum systems such as electronic spins [2–4], nuclear spins [5], and superconducting islands [6] are among the most promising candidates for realization of qubits. However, in contrast to isolated atomic systems [7], these solid-state qubits couple to a complex environment which often leads to rapid loss of coherence, and, in general, is difficult to understand [8, 9] For example, in contrast to identical atoms, solid-state qubits often behave differently from each other even within the same sample, under nominally identical conditions.

In what follows we describe a series of experiments in which we make use of coherent manipulation of a single electron solid-state quantum bit to obtain a detailed understanding of its local environment. Specifically, we demonstrate that electron spin coherence of a single nitrogen-vacancy (NV) center in high purity diamond sample is determined by interactions with ^{13}C nuclear spins. We show that under certain conditions the single electron spin dynamics is driven by coherent coupling to individual, proximal nuclear spins. The proximal nuclear spins can be addressed and controlled individually due to quantum back-action from the electron, which modifies their energy levels and magnetic moments. We demonstrate that this effect can be used for coherent manipulation of individual, isolated nuclear spins, which provide an excellent, long-term quantum memory even at room temperature. As an outlook, we discuss a new approach for building a scalable system starting from the coupled electron-nuclear spin qubit registers.

CP869, *AtomicPhysics 20, XX International Conference on Atomic Physics; ICAP 2006,*
edited by C. Roos, H. Häffner, and R. Blatt

THE MESOSCOPIC ENVIRONMENT OF A SINGLE ELECTRON SPIN

The Nitrogen Vacancy center in diamond

The NV center stands out among solid state systems because its electronic spin can be efficiently prepared, manipulated, and measured with optical and microwave excitation. Moreover, the stiff, mostly spinless diamond lattice permits long spin coherence times even at room temperature [2]. A spin triplet in its electronic ground state, the NV center exhibits a 2.87 GHz zero-field splitting which defines the $\hat{z}$ axis of the electron spin (see Fig. 1(a)). Application of a small magnetic field splits the $m_s = \pm 1$ states, allowing selective microwave excitation of a single spin transition. Under optical excitation at 532 nm, the fluorescence rate is stronger from the $m_s = 0$ than the $m_s = \pm 1$ states, allowing measurement of the electron spin state. Continued optical excitation relaxes the electron spin state, and leads to a net spin polarization in the $m_s = 0$ state [2].

In our experiments single NV centers are isolated and addressed at room temperature using optical scanning confocal microscopy (Fig. 1(b)) with excitation at 532 nm and fluorescence detection over the range 650-800 nm. Each circled spot is a single NV center, which is verified by photon correlation measurements (inset). We have investigated over 20 individual centers in detail, and where relevant we will indicate which center we observe. The 532 nm excitation polarizes the spin triplet into the $m_s = 0$ state on the timescale of a few microseconds. Following microwave manipulation of the spin, we detect the remaining population in the $m_s = 0$ state by again applying the excitation laser. Just after turning on the 532 nm light, the $m_s = 0$ state fluoresces more strongly than the $m_s = \pm 1$ states, allowing measurement of the spin (see Fig. 1(c)). Fig. 1(d) shows the oscillations in fluorescence which occur as a function of the duration of a microwave pulse resonant with the $m_s = 0$ to $m_s = 1$ transition [2]. These Rabi nutations should correspond to complete population transfer within the two-state system. Fluorescence data are thus normalized in units of $m_s = 0$ probability p, where $p = 1$ ($p = 0$) corresponds to the maximum (minimum) fluorescence in a fit to Rabi oscillations observed under the same conditions.

Spin echo spectroscopy of mesoscopic environment

To probe coherence properties of single electron spins we make use of Ramsey spectroscopy and spin echo techniques. Consistent with earlier observations [2], we find that the free electron spin precession (Ramsey signal) dephases on a timescale $T_2^* = 1.7 \pm 0.2\,\mu$s (Fig. 1(e)). The complex oscillation pattern observed suggests that a complicated non-Markovian environment is at the origin of the spin dynamics [10]. To gain further insight into the origin of electron spin dynamics, the spin-echo (or Hahn echo) sequence is used. It consists of the pulse sequence $\pi/2 - \tau - \pi - \tau' - \pi/2$, where π represents a microwave pulse of sufficient duration to flip the electron spin, and τ, τ' are durations of free precession intervals (see Fig. 2(a)). When the two wait times are equal, $\tau = \tau'$, this sequence decouples the spin from an environment that changes slowly

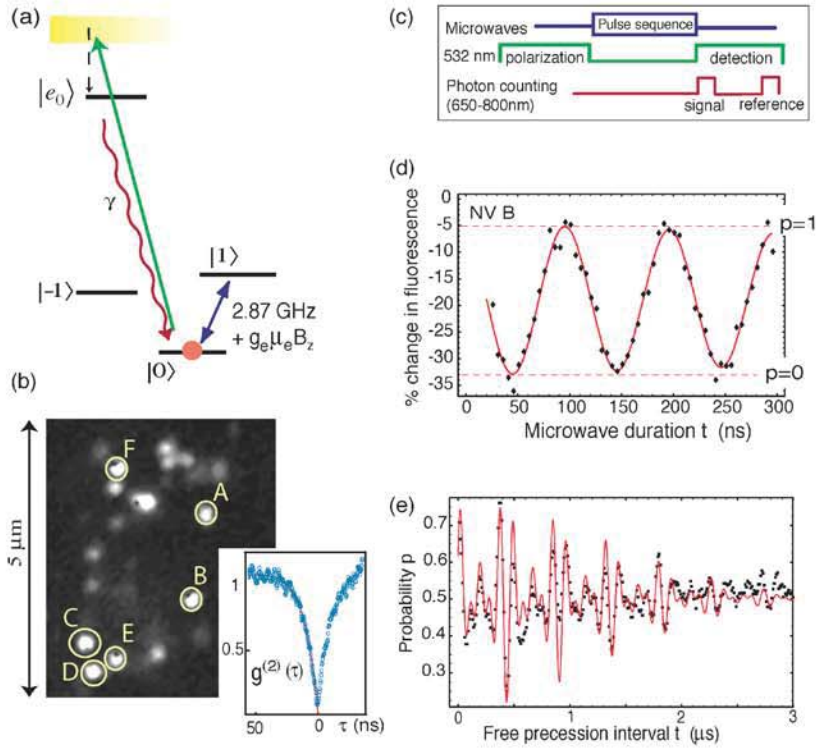

FIGURE 1. (a) The energy level structure of the NV center. (b) Scanning confocal image showing locations of single NV centers A-F. The inset shows a representative measured auto-correlation function $g^{(2)}(\tau)$ from a single NV, where $g^{(2)}(0) \ll \frac{1}{2}$ indicates that we are exciting a single quantum emitter. (c) Experimental procedure. (d) Driven spin oscillations (Rabi nutations). The percent change in fluorescence between the signal and reference is observed as a function of resonant microwave pulse duration (inset) for NV B. (e) Electron spin free precession. The data was taken with a microwave detuning of 8 MHz, as a function of delay between the two $\pi/2$ pulses (inset). The Ramsey signal was fitted (red) to $\exp(-(t/T_2^*)^2)\sum_{i=1}^{3}\cos(2\pi f_i t)$, where f_i correspond to the level shifts from the host ^{14}N nuclear spin, obtaining $T_2^* = 1.7 \pm 0.2\mu$s.

compared to τ. A typical Hahn echo signal (center B) in low magnetic field $B = 5$ Gauss is displayed in Fig. 2(b). The spin echo yields a much longer coherence time $\tau_C \approx 13 \pm 0.5\mu\text{s} \gg T_2^*/2$, thus indicating a long correlation time associated with the electron spin environment.

Spin-echo spectroscopy also provides a useful tool for understanding a non-Markovian environment: by observing the spin-echo peak ($\tau = \tau'$) under varying conditions, we can indirectly determine the response of the environment, and from this glean details about the environment itself. In particular, we observe that the echo signal depends greatly on magnetic field. As magnetic field is increased, the initial decay of the spin echo signal occurs faster and faster; but at longer times $\tau = \tau_{\mathbf{R}}$ the spin echo revives. Fig. 2(c) shows a typical spin echo signal (center B) in moderate magnetic field as a function of time $\tau = \tau'$. The initial collapse of the signal is followed by periodic revivals extending out to $2\tau \sim 242\mu$s. We find that both the collapse and revival rates

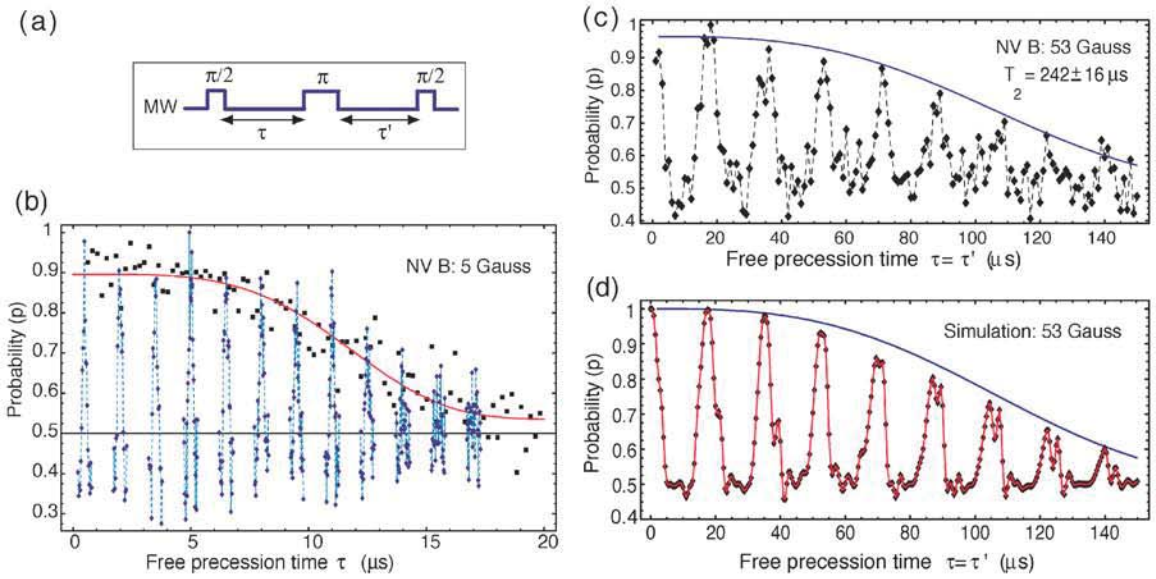

FIGURE 2. (a) Spin echo. The spin-echo pulse sequence. A single spin-echo is observed by holding τ fixed and varying τ'. (b) Spin echo decay for NV B in a small magnetic field (B $\sim$ 5 G). Individual echo peaks are mapped out by scanning τ' for several values of τ (blue curves). The envelope for the spin echoes (black squares), which we refer to as the spin-echo signal, maps out the peaks of the spin echoes. It is obtained by varying τ and τ' simultaneously, so that $\tau = \tau'$ for each data point. The spin-echo signal is fitted to $\exp(-(\tau/\tau_C)^4)$ (red curve) to obtain the estimated coherence time $\tau_C = 13 \pm 0.5\mu$s . (c) Collapse and revival of the spin-echo signal from NV B in a moderate magnetic field (53 Gauss). The decay of the revivals (blue curve) is found by fitting the height of each revival to $\exp(-(2\tau/T_2)^3)$, as would be expected from ^{13}C dipole-dipole induced dephasing [13], with $T_2 \approx 242 \pm 16\mu$s. (d) Simulation of collapse and revival for an NV center in 53 Gauss applied magnetic field, surrounded by a random distribution of 1.1% ^{13}C spins (see [12] for detail). Additional structure in the simulation arises from coherent interactions with the nearest ^{13}C in the lattice, via the same mechanism shown in Fig. 4. The phenomenological decay is added to the simulation for comparison with experimental data.

depend strongly on the magnetic field amplitude, but not its orientation, and do not vary significantly between NV centers (data not shown). Furthermore, the revival rate $1/\tau_R$ precisely matches the Larmor precession frequency for ^{13}C nuclear spins, as shown in Fig. 3(a).

These results can be understood qualitatively by considering a single NV spin surrounded by a bath of ^{13}C nuclear spins, as illustrated in Fig. 3(b). A natural diamond lattice consists of 98.9% spinless ^{12}C atoms interspersed with 1.1% of randomly distributed spin-1/2 ^{13}C nuclei. Each nuclear spin $I^{(j)}$ interacts with the electron spin S via the dipole interaction, contributing to an effective magnetic field at the site of the NV center. In an external magnetic field, the large 2.87 GHz quadrupole splitting inhibits electron spin transitions, but the spin-1/2 nuclear spins are free to precess at the Larmor frequency $\mu_n B$, where $\mu_n = 1.071$ kHz/G. When the Larmor period is shorter than the spin echo time τ, the ^{13}C spins can no longer be treated as quasi-static. Their precession induces periodic decorrelation and rephasing of the nuclear spin bath, which leads to collapses and revivals of the electron spin echo signal shown in Fig. 2(c) (upper). Thus, our observations clearly demonstrate that in finite magnetic field at times $2\tau < 200\mu$s,

the NV center coherence is governed primarily by interactions with ^{13}C nuclei.

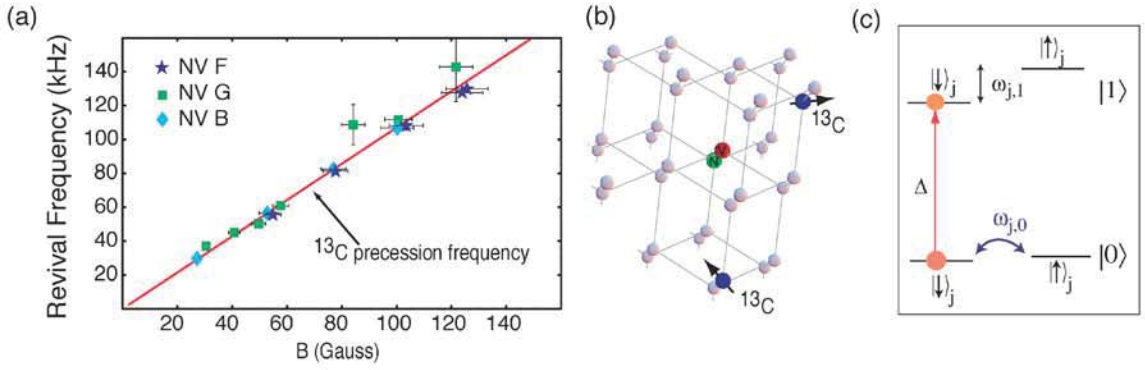

FIGURE 3. (a) Spin-echo revival frequency as a function of magnetic field amplitude. Data from three representative centers NV B, NV F, and NV G (not shown in Fig. 1(b)) exhibit revivals which occur with the ^{13}C Larmor precession frequency (red). The data points for NV B and F were taken with $B||\hat{z}$, while the data for NV G were taken in a variety of magnetic field orientations. (b) Illustration of the ^{13}C environment surrounding the NV center. (c) Physical model for spin-echo modulation.

COHERENT CONTROL OF COUPLED ELECTRON AND NUCLEAR SPIN QUBITS

Dynamics of electron-nuclear spin system

Every NV center studied exhibits spin-echo collapse and revival on long time scales, but many also showed more complicated evolution on short time scales. As an example, the signal from the center E is shown in Fig. 4(a). The oscillating signal has slow and fast components at ~ 0.6 MHz and ~ 9 MHz respectively. The fast component (referred to as the modulation frequency) is relatively insensitive to the magnetic field (Fig. 4(b)), but the slow component (envelope frequency) varies dramatically with the magnetic field amplitude and orientation (see Fig. 4(c)). These observations indicate the electron spin gets periodically entangled and disentangled with an isolated system, until the spin echo finally collapses from interactions with the precessing bulk spin bath. Although the data is not shown, some NV centers, for example NV C, exhibit several envelope and modulation frequencies, indicating that the electron spin interacts coherently with multiple ^{13}C nuclei. Other centers, for example NV F, show no evidence of proximal ^{13}C spins.

We begin with a simple treatment, which neglects the terms proportional to S_x, S_y because they are suppressed by the large electron spin splitting $\Delta \approx 2.87$ GHz (the so-called secular approximation [11]). In this model (Fig. 3(c)) the $m_s = 1$ nuclear spin states have a fixed hyperfine splitting $\omega_{j,1} \sim \mu_e \mu_n (< 1/r_j^3 > + 8\pi |\Psi_e(r_j)|^2/3)$, whereas the degenerate $m_s = 0$ nuclear spin states can precess in a small applied magnetic field at the bare ^{13}C Larmor frequency $\omega_{j,0} = \omega_0$. Here μ_e and μ_n are the electron and nuclear magnetic moments respectively, $|\psi_e(r_j)|^2$ is the electron spin density at the site of the nuclear spin, and brackets $<>$ denote an average over the electron wavefunction $\psi_e(r)$.

When we include many nuclear spins in the echo signal, the fast echo modulations $\omega_{j,1}$ interfere with each other, causing initial decay of the signal as $\exp[-(\tau/\tau_C)^4]$. However, when $\tau = \tau' = 2\pi/\omega_0$, the spin-echo signal revives. Simulations (Fig. 2(d)) are in good agreement with the observed collapses and revivals. For further details, see [12].

Such a simple picture cannot explain the observed echo modulation, however, because it predicts that the spin-echo signal should collapse before coherent interactions with individual ^{13}C spins become visible. In fact, the nonsecular terms in the Zeeman and dipole interactions slightly mix the electron spin levels, introducing some electronic character to the nearby nuclear spin levels, and thus augmenting their magnetic moment by $\sim \mu_e(\omega_{j,1}/\Delta)$. Since $\mu_e \gg \mu_n$, this greatly enhances the nuclear Larmor precession rate for nearby spins. Furthermore, the enhancement is anisotropic: it is strongest when the external field is oriented perpendicular to the NV axis, corresponding to the largest degree of mixing. For a properly oriented magnetic field, proximal nuclei can thereby entangle and disentangle with the NV spin on timescales much faster than the bare ^{13}C Larmor period.

These theoretical predictions are in good agreement with our observations (Fig. 4). In addition, by fitting the envelope frequency as a function of magnetic field, we are able to estimate the six coupling parameters which characterize the hyperfine interaction [12]. In principle, these parameters should also allow for precise determination of absolute nuclear position in the diamond lattice. However, direct comparison to the microscopic model depends sensitively on the details of the electronic wavefunction due to both the isotropic contact contribution and the averaged dipolar term. Our results indicate that both terms can be important.

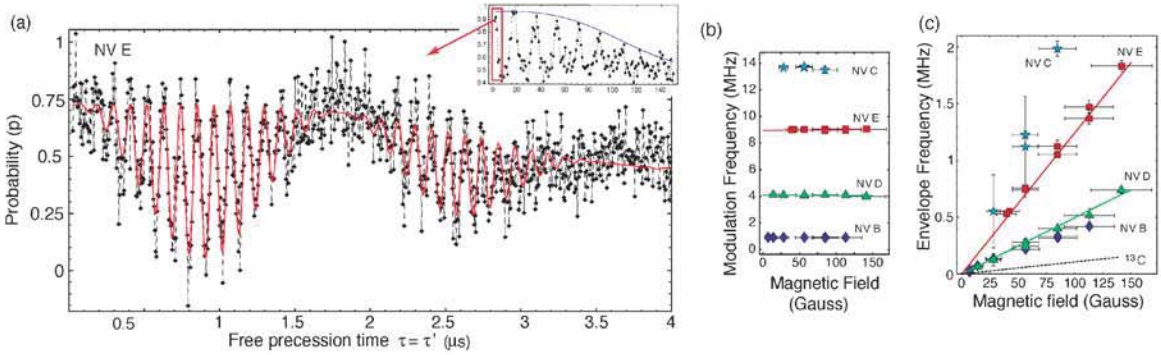

FIGURE 4. (a) Spin echo modulation as observed for NV E with B = 42 ±6 Gauss $||-\hat{x} + \hat{z}$. The red curve represents a theoretical fit with the expected functional form $\exp(-(\tau/\tau_C)^4)\left(a - b\,\sin(\omega_0\tau/2)^2 \sin(\omega_1\tau/2)^2\right)$, yielding the modulation frequency $\omega_0 \sim 2\pi$ 9 MHz and envelope frequency $\omega_1 \sim 2\pi$ 0.6 MHz. (b) Modulation frequency for NV B-E as a function of magnetic field B $|| -\hat{x} + \hat{z}$. (c) Envelope frequency, same conditions as (b). The envelope frequencies are different for each center, but they all exceed the bare ^{13}C Larmor precession frequency (dashed line).

Coherent control of single nuclear spins

Most recently we have shown [14] that electron spin manipulation can be used to coherently prepare and control individual nuclear spins in the diamond lattice. To accomplish this, a technique was developed for mapping the electronic coherence of a single NV center to a proximal nuclear spin. As illustrated in Fig. 5(a),(b), this technique involves a selective rotation of the electron spin, conditional on the state of nuclear spin, followed by free nuclear spin precession. Specifically, a selective microwave π-pulse is used to flip the states $|m_s = 0, \downarrow\rangle \leftrightarrow |m_s = 1, \downarrow\rangle$, implementing a mapping operation between the nuclear and electron spin states. This is followed by a period of free evolution $\pi/\omega_{j,0}$ in which the states $|m_s = 0, \uparrow\rangle \leftrightarrow |m_s = 0, \downarrow\rangle$ due to Larmor precession. Subsequent polarization of the electron spin prepares the system in $|m_s = 0, \downarrow\rangle$. Fig. 5(c) shows Larmor precession signal from a single ^{13}C nuclear spin. This data is obtained by the composite pulse sequence shown in Fig. 5(b), consisting of a mapping sequence, polarization, free nuclear evolution, and mapping from the nuclear state back to the electron state for measurement. Our data demonstrate combined nuclear spin preparation and readout fidelity of 85%. From the known coupling constants, we estimate that the nuclear spin qubit storage times approaching seconds may eventually be obtained.

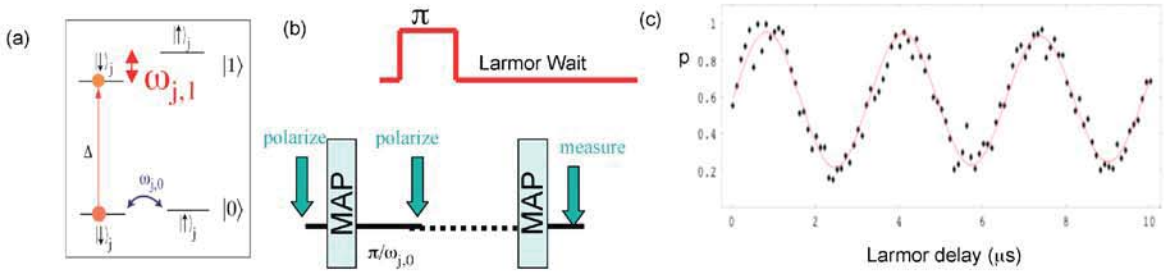

FIGURE 5. Observation of coherent free precession of an individual, isolated nuclear spin in diamond. (a) Energy level scheme depicting the coupled electron-nuclear spin system. The arrow depicts the resonance to which the microwave oscillator is tuned. Here, $\omega_{j,1}$ is the splitting due to the field from the electron spin on the nucleus, and $\omega_{j,0}$ is the Larmor frequency due to the applied magnetic field. (b) A simple mapping sequence from nuclear to electron spin (top), with a composite pulse sequence for polarizing nuclear spin (bottom). (c) Precession signal from a single nuclear spin, demonstrating a state preparation fidelity $\sim 85\%$.

OUTLOOK

In this section, we discuss a new approach for building a scalable system starting from the coupled electron-nuclear spin qubit registers. In our approach small registers, placed at arbitrary locations and consisting of few proximally coupled quantum bits, are coupled to each other by quantum optical communication channels that can be used to establish long-range entanglement and perform remote operations between distant quantum bits. The individual quantum nodes can be constructed from electron-spin selective, single photon emitters in solid-state systems [15]. The electron spin can be used for the preparation and manipulation of proximal nuclear spins and for entanglement with other

nodes. The spin degrees of freedom of proximal nuclei can be used for long-term storage of the quantum information.

For example, we recently proposed and analyzed a novel method that uses fixed, minimal physical resources to achieve generation and nested purification of quantum entanglement for quantum communication over arbitrarily long distances [15, 16]. In this method, we use single photon emitters with two internal degrees of freedom formed by an electron spin and a nuclear spin to build intermediate nodes in a quantum channel. State-selective fluorescence can be used for probablistic entanglement generation between electron spins in adjacent nodes. We analyzed several approaches which are applicable to realistic, homogeneously broadened single photon emitters such as NV centers, indicating that long-range entanglement is feasible. Furthermore, the coupled electron and nuclear spins can be used to efficiently implement entanglement swapping and purification. We showed, in particular, that these techniques can be combined to generate high-fidelity entanglement over arbitrarily long distances. A specific protocol can be designed that functions in polynomial time and tolerates percent-level errors in entanglement fidelity and local operations. This example illustrates the potential power of an optically coupled few-qubit system with a long instrinsic memory.

In conclusion, we have demonstrated that techniques developed in AMO physics can be used to quantify the mesoscopic nuclear spin environment of single electron spins in the solid state. Furthermore, they allow us to selectively address and manipulate single nuclear spins. Such nuclear spins could be used as a resource for long-term storage of quantum information. They can be effectively manipulated via nearby electronic spins and potentially coupled together using quantum optical techniques to explore a variety of proposed quantum information systems.

ACKNOWLEDGMENTS

We are grateful to John Doyle and Doyle Lab members for making these experiments possible. We thank A. Mukherjee, N. Khaneja, E. Demler, C. Marcus, and S. Sachdev for many stimulating discussions and experimental help, and S.Prawer for providing high-purity diamond samples. This work was supported in part by the NSF Career Award, ARO MURI, and the Packard, Sloan, and Hertz Foundations. FJ and JW acknowledge support from DFG (SFB/TR21) and the European Commission (QAP).

REFERENCES

1. D. P. DiVincenzo, *Science* **270**, 255 (1995).
2. For review see F. Jelezko, J. Wrachtrup, e-print:quant-ph/0510152 (2005).
3. J. R. Petta *et al.*, *Science* **309**, 2180 (2005).
4. M. Atature *et al.*, *Science* **312**, 551 (2006).
5. B. E. Kane, *Nature* **393**, 133 (1998).
6. Y. Makhlin, G. Schon, A. Shnirman, *Rev. Mod. Phys* **73**, 357 (2001).
7. J.I. Cirac, P. Zøller, *Physics Today* **57**, 38 (2004).
8. A. V. Khaetskii, D. Loss, L. Glazman, *Phys. Rev. Lett.* **88**, 186802 (2002).
9. R. de Sousa, S. Das Sarma, *Phys. Rev. B* **68**, 115322 (2003).

10. Detailed interpretation of the Ramsey fringes requires including both the 8MHz detuning of the applied microwaves and the hyperfine levels of the native $I = 1$ ^{14}N which forms the NV center. However, the details of the ^{14}N hyperfine interaction will not affect spin-echo spectroscopy, since the three ^{14}N hyperfine detunings are echoed away. More importantly, the ^{14}N nucleus has a large quadrupole splitting P that effectively prevents precession between the nuclear sub-levels. Hence, for fields $B \ll P/(g_n\beta_n) \sim 1.64$ T, we may neglect the effect of the ^{14}N nucleus on spin-echo signals.
11. A. Schweiger, G. Jeschke, *Principles of pulse electron paramagnetic resonance* (Oxford University Press, Oxford UK, 2001).
12. L. Childress, *et al.*, *accepted for publication in Science*.
13. C.P. Slichter, *Principles of magnetic resonance* (Springer-Verlag, New York, 1990).
14. M. V. Gurudev Dutt, *et al.*, *in preparation*.
15. L. Childress, J.M. Taylor, A.S. Sørensen, M.D. Lukin, *Phys. Rev. Lett.* **96**, 070504 (2006).
16. L. Childress, J.M. Taylor, A.S. Sørensen, M.D. Lukin, *Phys. Rev. A* **72**, 052330 (2005).